

PROCEEDINGS OF SPIE

[SPIDigitalLibrary.org/conference-proceedings-of-spie](https://spiedigitallibrary.org/conference-proceedings-of-spie)

The Giant Magellan Telescope adaptive optics program

Bouchez, Antonin, Acton, D. , Biasi, Roberto, Conan, Rodolphe, Espeland, Brady, et al.

Antonin H. Bouchez, D. Scott Acton, Roberto Biasi, Rodolphe Conan, Brady Espeland, Simone Esposito, Josema Filgueira, Daniele Gallieni, Brian A. McLeod, Enrico Pinna, Fernando Santoro, Gelys Trancho, Marcos A van Dam, "The Giant Magellan Telescope adaptive optics program," Proc. SPIE 9148, Adaptive Optics Systems IV, 91480W (21 July 2014); doi: 10.1117/12.2057613

SPIE.

Event: SPIE Astronomical Telescopes + Instrumentation, 2014, Montréal, Quebec, Canada

The Giant Magellan Telescope Adaptive Optics Program

Antonin H. Bouchez^{1a}, D. Scott Acton^b, Roberto Biasi^c, Rodolphe Conan^d, Brady Espeland^a, Simone Esposito^c, Josema Filgueira^a, Daniele Gallieni^f, Brian A. McLeod^g, Enrico Pinna^e, Fernando Santoro^a, Gelys Trancho^a, Marcos A. van Dam^h

^aGMTO Corp., 251 S. Lake Ave., Pasadena, CA, USA 91101; ^bBall Aerospace & Technologies Corp, 1600 Commerce St., Boulder, CO, USA 80306; ^cMicrogate Srl., Via Antonio Stradivari 4, 89100 Bolzano, Italy; ^dResearch School of Astronomy and Astrophysics, The Australian National University, Cotter Road, Weston, ACT, Australia 2611; ^eOsservatorio Astrofisico di Arcetri, Largo Enrico Fermi 5, 50125 Firenze, Italy; ^fA.D.S. International Srl., Via Roma 87, 23868 Valmadrera Lecco, Italy; ^gSmithsonian Astrophysical Observatory, 60 Garden St., Cambridge, MA, USA 02139; ^hFlat Wavefronts, P.O. Box 1060, Christchurch, New Zealand 8140

ABSTRACT

The Giant Magellan Telescope (GMT) adaptive optics (AO) system will be an integral part of the telescope, providing laser guidestar generation, wavefront sensing, and wavefront correction to every instrument currently planned on the 25.4 m diameter GMT. There will be three first generation AO observing modes: Natural Guidestar, Laser Tomography, and Ground Layer AO. All three will use a segmented adaptive secondary mirror to deliver a corrected beam directly to the instruments.

The Natural Guidestar mode will provide extreme AO performance, with a total wavefront error less than 185 nm RMS using bright guidestars. The Laser Tomography mode uses 6 lasers and a single off-axis natural guidestar to deliver better than 290 nm RMS wavefront error at the science target, over 50% of the sky at the galactic pole. The Ground Layer mode uses 4 natural guidestars on the periphery of the science field to tomographically reconstruct and correct the ground layer AO turbulence, improving the image quality for wide-field instruments. A phasing system maintains the relative alignment of the primary and secondary segments using edge sensors and continuous feedback from an off-axis guidestar. We describe the AO system preliminary design, predicted performance, and the remaining technical challenges as we move towards the start of construction.

Keywords: Extremely Large Telescopes, Adaptive Optics, Adaptive Secondary Mirrors, Ground Layer AO

1. INTRODUCTION

The Giant Magellan Telescope is a 25.4 m diameter optical/infrared telescope being developed for the purpose of conducting forefront scientific research in general astrophysics, cosmology, and the study of extrasolar planetary systems¹ (Figure 1). The GMT optical design is a fast, wide field (20' diameter) aplanatic Gregorian with a plate scale of 0.99 arcsec/mm at the final f/8.2 focus². The optics are supported in an altitude-azimuth structure that has been designed to be stiff and compact. The primary mirror will be composed of seven 8.4 m diameter borosilicate honeycomb segments fabricated by the Stewart Observatory Mirror Lab. Two secondary mirror assemblies with the same optical prescription will be provided for the GMT: an adaptive secondary mirror (ASM) and a fast-steering secondary mirror (FSM). Each consists of seven 1.05 m diameter segments supported by 6 degree of freedom positioning systems from a rigid top end frame. The ASM will be used in routine operation to support all the telescope observing modes, while the FSM will be used during commissioning and whenever servicing of the ASM is required.

Science instruments will mount on the moving structure of the telescope, utilizing either the direct Gregorian focus (2 reflections), or a folded Gregorian focus provided by a steerable M3 located below the primary mirror (3 reflections). Narrow-field AO instruments will be located at the folded Gregorian focus, while instruments with a field of view up to 20' diameter will be located at the direct Gregorian focus. Up to 11 instruments can be accommodated on the telescope simultaneously, most mounted on a single large Gregorian Instrument Rotator (GIR) which provides field de-rotation.

¹ abouchez@gmto.org; phone +1 626 204 0517; <http://www.gmto.org>

The preliminary design of the first generation of instruments is underway, and a call for proposals for second-generation instrument concepts is planned in 2015³. Two of the first generation instruments will be narrow-field infrared imagers/spectrographs designed specifically to take advantage of the diffraction-limited NGAO and LTAO observing modes (GMTIFS⁴ and GMTNIRS⁵). The wide-field multi-object GMACS spectrograph⁶ and the single-object, high-resolution GCLEF spectrograph⁷ will both benefit from GLAO correction.

The GMT will be located on Cerro Campanas at Las Campanas Observatory in Chile. The summit of Cerro Campanas has been leveled in preparation for construction, to an elevation of 2518 m above sea level. A rotating enclosure will shield the telescope from the elements in daytime, and from wind and moonlight at night. A summit support building located 100 m away provides facilities for operating and maintaining the telescope, instruments, and AO system components⁸. The GMT site provides excellent astronomical conditions, with over 220 photometric nights per year and a median Fried parameter $r_0=16.4$ cm. The site is however quite windy, with a median nighttime wind speed of 6.3 m/s.

The following section describes the GMT AO observing modes, performance requirements, and architectural choices. Section 3 presents the preliminary design of the major AO subsystems. Section 4 summarizes the predicted performance of the system, and Section 5 presents our conclusions.

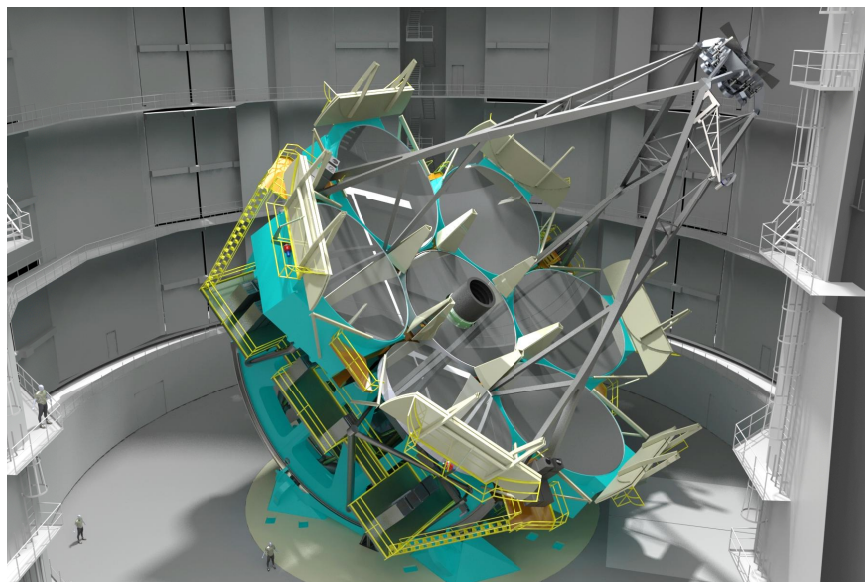


Figure 1. The Giant Magellan Telescope in its enclosure.

2. REQUIREMENTS AND ARCHITECTURE

2.1 Observing Modes

The GMT will support three AO observing modes for the first generation of instruments, using different wavefront sensing approaches to balance turbulence compensation with sky coverage and field of view. The ASM is the primary wavefront corrector for all of these modes.

- The Ground Layer AO (GLAO) observing mode uses natural guidestars (NGS) in the periphery of the direct Gregorian field of view to tomographically reconstruct the turbulence below ~ 1 km altitude, providing modest image quality improvement at $0.35\text{-}25$ μm over a field of view up to 20 arcmin diameter.
- The Natural Guide Star AO (NGAO) observing mode uses a single NGS wavefront sensor located ahead of the instrument to provide all of the wavefront correction information for the AO System, delivering diffraction-limited imaging at $0.9\text{-}25$ μm wavelength over a field of view limited by atmospheric anisoplanatism.
- The Laser Tomography AO (LTAO) observing mode uses a $1'$ diameter asterism of 6 Laser Guidestars (LGS) to tomographically reconstruct the high-order components of the atmospheric wavefront aberrations in the direction of a central science target. One NGS is used to measure tip-tilt, focus, segment piston, and dynamic

calibration terms. Wavefront aberration will be compensated by the ASM, providing diffraction-limited imaging at 0.9-25 μm wavelength over a field of view limited by atmospheric anisoplanatism.

The ASM must also support the Natural Seeing (NS) observing mode, in which only fast tip-tilt is corrected. The AO observing modes will be deployed sequentially during the commissioning period of the telescope, with the system first supporting GLAO correction for the GCLEF and GMACS instruments, then NGAO mode and finally LTAO mode for the diffraction-limited instruments. Second-generation observing modes which use the ASM as the first-stage corrector for an extreme, multi-conjugate, or multi-object AO system are being considered.

2.2 Performance Requirements and Error Budgets

The top-level performance requirements in each observing mode are listed in Table 1. The GMT AO performance requirements have deliberately been kept somewhat less ambitious than those of other extremely large telescope projects, allowing a comparatively simple and cost-effective design to meet those requirements. In addition to diffraction-limited and high-contrast science, there is a strong scientific emphasis on spectroscopy of low surface-brightness objects.

All requirements are specified at 15° from zenith in median integrated turbulence conditions ($r_0=16.4$ cm at zenith), but with 75th percentile wind conditions (10 m/s), seasonal minimum sodium density (2.1×10^{13} atoms m^{-2}) and a conservative assumption of the turbulence outer scale ($L_0=60$ m). The turbulence profile used is the January 2008 “typical-typical” model of Goodwin⁹, measured using the SLODAR method on the 2.5 m DuPont telescope.

Mode	Performance Requirements
GLAO	SCI-1887: <0.30 arcsec FWHM at K band over >6.5 arcmin diameter, $>50\%$ of the time
NGAO	SCI-1883: $>75\%$ K ($2.18 \mu\text{m}$) Strehl for $R < 8$ stars SCI-1882: $>10^5$ contrast at 0.12 arcsec ($4\lambda/D$) in L' band
LTAO	SCI-1884: $>30\%$ H ($1.65 \mu\text{m}$) Strehl over 20% of the sky at the galactic pole SCI-1885: $>40\%$ K ($2.18 \mu\text{m}$) ensquared energy in 50×50 mas over 50% of sky at the galactic pole SCI-1886: $>50\%$ K ($2.18 \mu\text{m}$) ensquared energy in 85×85 mas with a $K=15$ on-axis NGS

Table 1: GMT AO performance requirements

Error budgets based on simple analytic calculations and confirmed using numerical simulations have been developed to flow down the top-level AO performance requirements to those of subsystems and components. The starting point for analytic performance estimates is the GMT diffraction-limited PSF. The gaps in the GMT pupil result in diffraction features which have a significant impact on encircled/ensquared energy performance metrics, and a modest impact on FWHM. The on-axis pupil ASM pupil and a simulated NGAO PSF are illustrated in Figure 2. The apparent holes in the outer segments are projections of holes in the ASM face sheets, required to accommodate their central flexures.

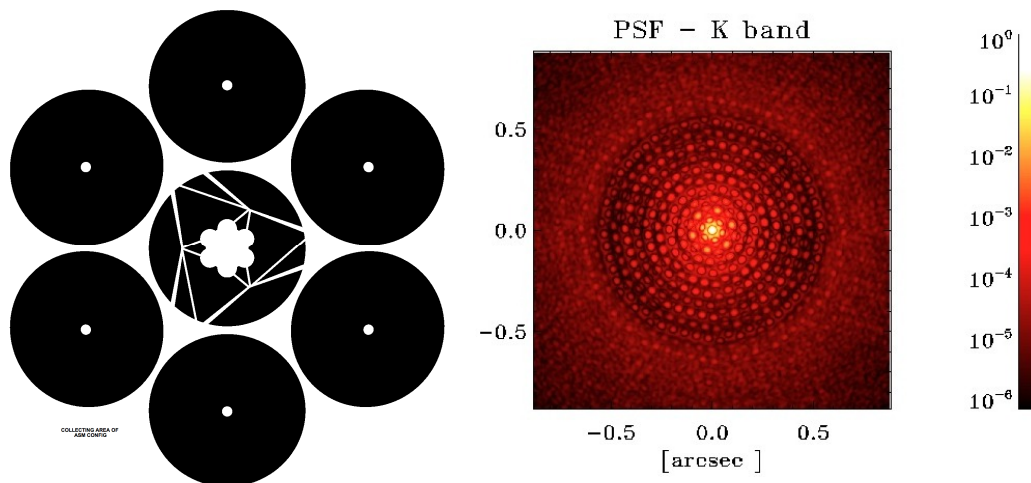


Figure 2. (Left) GMT on-axis pupil. (Right) Simulated NGAO mode PSF with 91% K Strehl (logarithmic stretch).

The ASM actuator density is driven by NGAO observing mode requirements, and its conjugate height of 160 m above ground is dictated by the aplanatic Gregorian optical design. The GLAO mode performance is therefore determined by the wavefront sensor design, reconstruction algorithms, and of course the turbulence height distribution. While an analytic error budget for a median turbulence profile has been developed, it has proven less useful than those for the diffraction-limited observing modes. We have instead relied on wave-optics simulations using random guidestar asterisms and random draws from a set of measured turbulence profiles¹⁰ to optimize the system design and characterize its expected performance.

To meet the Strehl and contrast requirements, the NGAO mode must maintain <170 nm RMS high-order wavefront error and <1.85 mas RMS tip-tilt error when using bright guidestars. This requirement has been flowed down to individual sources of wavefront error as indicated in Table 2. Meeting these allocations requires an actuator spacing in the pupil of <30 cm, wavefront sensor framerate >700 Hz, and an on-instrument “truth” wavefront sensor to detect slowly-varying errors not sensed by the NGAO wavefront sensor.

The LTAO performance requirements are challenging, both in terms of high-order wavefront error and sky coverage. The flowdown to individual sources of wavefront error for 20% sky coverage at the galactic pole is shown in Table 2. Maintaining the high-order wavefront error below 260 nm RMS using available guidestar lasers requires an asterism of six LGS, accurate tomography algorithms, and an on-instrument truth wavefront sensor. The <3.0 mas RMS tip-tilt error requirement is particularly challenging to meet in the presence of the ~10 mas RMS telescope wind shake expected in 75th percentile wind conditions when the enclosure is in the minimum aperture configuration¹¹. The system design achieves this level of tip-tilt control using a single diffraction-limited tip-tilt sensor within the instrument, operating in the K band at 500 Hz frame rate.

Error Term	NGAO mode, V=8			LTAO mode, 20% sky @ b=90		
High-order error [nm]	170 / 105			260 / 209		
AO high-order aberrations		108 / 65			202 / 185	
Atmospheric fitting			65 / 60			105 / 105
Temporal bandwidth			60 / 20			50 / 50
HO WFS measurement			55 / 14			50 / 30
HO aliasing			30 / 10			40 / 35
Tomography						100 / 90
Focus						35 / 35
Dynamic calibration						45 / 45
Atmospheric Piston						100 / 85
Telescope Segment Piston		45 / 10			65 / 35	
AO calibration		62 / 62			76 / 74	
TS calibration			35 / 35			35 / 35
LTWS calibration			35 / 35			30 / 30
Instrument Window (reflection)			20 / 20			20 / 20
LGS Fold Optic (reflection)			20 / 20			20 / 20
Pupil alignment on WFS			25 / 25			45 / 41
Field-dependent aberrations						30 / 30
Uncorrectable telescope aberrations		30 / 15			30 / 15	
Uncorrectable instrument aberrations		50 / 50			50 / 50	
Contingency		89			115	
Image motion error [mas]	1.85 / 1.37			3.00 / 2.34		
AO Fast Tip-tilt errors		1.60 / 1.34			2.55 / 2.25	
Tip-tilt measurement			0.50 / 0.10			1.00 / 0.80
Tip-tilt temporal bandwidth			0.50 / 0.17			1.00 / 0.80
Tip-tilt aliasing			0.25 / 0.20			0.50 / 0.40
Tip-tilt anisokinetism						1.50 / 1.35
Residual windshake			1.00 / 0.85			1.00 / 0.90
Residual mechanical vibrations			1.00 / 1.00			1.00 / 1.00
AO Slow tip-tilt errors		0.28 / 0.26			0.28 / 0.23	
Residual atmospheric dispersion			0.20 / 0.20			0.20 / 0.20
Residual flexure during exposure			0.20 / 0.17			0.20 / 0.12
GIR rotation error					0.60 / 0.60	
Contingency		0.88			1.44	

wavelength [μm]	1.22	1.65	2.18	1.22	1.65	2.18
FWHM [mas]	10.7 / 10.7	14.5 / 14.4	19.0 / 18.9	11.0 / 10.8	14.7 / 14.5	29.2 / 19.1
Strehl ratio	0.40 / 0.68	0.60 / 0.81	0.75 / 0.89	0.11 / 0.25	0.30 / 0.46	0.50 / 0.64
Ensquared energy in 50x50 mas	0.37 / 0.59	0.48 / 0.62	0.53 / 0.61	0.14 / 0.25	0.28 / 0.39	0.40 / 0.47

Table 2: Wavefront error budgets and performance estimates corresponding to requirements SCI-1883 (K Strehl >0.75 in NGAO mode with V=8 guidestar) and SCI-1884 (H Strehl >0.30 in LTAO mode with 20% sky coverage at the galactic pole). The first number in each cell is the requirement, while the second is the estimated performance of the preliminary design. Values in blue are allocations for cases in which the design performance has not yet been determined.

2.3 AO System Architecture

The GMT AO system architecture is based around an ASM as the primary wavefront corrector. When combined with a “direct feed” of the high-order wavefront sensors, this choice naturally provides high throughput, low emissivity, a wide corrected field of view, and low differential aberrations between the wavefront sensors and instruments. The direct-feed wavefront sensing architecture is so named because light from the telescope is passed directly from the tertiary mirror (M3) to the science instrument operating in the NGAO and LTAO modes. High-order wavefront sensing is performed using visible light reflected from a dichroic instrument window tilted 20° to the incoming beam. An on-instrument NGS wavefront sensor (OIWFS) measures additional low-order or low temporal frequency errors to which the visible wavefront sensors are blind (Figure 3).

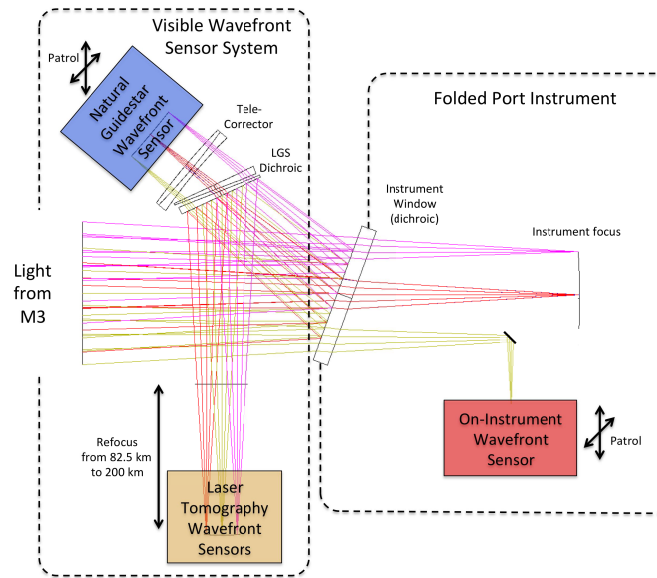


Figure 3. Schematic of the direct feed architecture, as implemented in the GMT AO system design.

The direct feed architecture requires that the visible wavefront sensors be replicated for each instrument, but the additional cost is compensated by the opportunity to tailor each set of sensors to the instrument’s science case (for example, the diameter of the LGS asterism). Flexure between the visible wavefront sensors and the instrument focal plane is sensed by the OIWFS inside the instrument cryostat. The OIWFS must also sense fast tip-tilt, focus, and segment piston error in the LTAO mode.

Wavefront sensing in the GLAO mode will be provided by the Acquisition, Guiding, and Wavefront sensing System (AGWS) probes, which patrol the periphery of the direct Gregorian focal plane (Figure 4). An extensive trade study comparing this NGS sensing architecture to one using laser guide stars was performed during the preliminary design phase^{12,13}. The NGS GLAO system was selected based on its higher throughput and observing efficiency and far lower cost. In the GLAO mode, the wavefront of four natural guide stars will be sensed by the AGWS at up to 200 Hz, the ground layer turbulence will be tomographically reconstructed from these signals, and then corrected by the ASM. GLAO correction will thus be available to any instrument on the telescope, regardless of focal station, whenever the ASM is installed.

Achieving the diffraction limit of the 25.4 m aperture of the GMT will require the primary and secondary mirrors to be phased to <65 nm rms. Due to the large separation between primary segments (30-40 cm) and their construction of borosilicate glass, which has a non-zero CTE, capacitive or inductive edge sensors alone are not expected to be sufficiently stable over timescales longer than a few minutes. In the NGAO observing mode, the natural guide star wavefront sensor can sense and correct segment piston at up to 2 kHz. However, only faint natural guide stars are generally available in the LTAO mode. The GMT therefore uses a 3-stage phasing system consisting of a coarse optical phasing sensor with a large capture range to initially phase the telescope, primary and secondary mirror edge sensors to maintain alignment over short timescales, and a high-sensitivity optical sensor to correct long-term drifts in the edge sensors. Since the primary and secondary segments are matched one-to-one, errors can be rapidly compensated using

the agile adaptive secondary mirror, then off-loaded to the primary or secondary segment positioning actuators as appropriate.

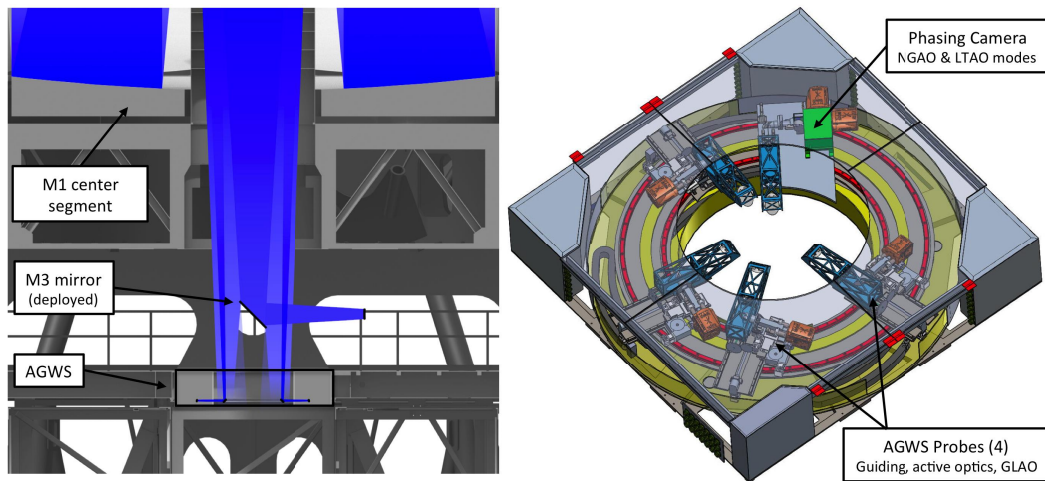


Figure 4. (Left) Cross-section of the telescope showing the location of the AGWS sensors. (Right) The AGWS unit viewed from below, with 4 patrolling guiding and wavefront sensing probes and one phasing camera.

3. AO SYSTEM DESIGN

3.1 Adaptive Secondary Mirror

The segmented GMT optical design leads to specifications for each ASM segment that are similar to those of present-generation adaptive mirror telescopes (e.g., the Large Binocular Telescope¹⁴, Magellan Telescope¹⁵, and ESO Very Large Telescope¹⁶). The ASM benefits greatly from the design heritage of those mirrors, and represents the 4th generation of such devices designed by a consortium of Microgate Corp. and ADS International.

Each 1.05 m diameter ASM segment has 672 voice coil actuators, supporting a 2 mm thick Zerodur face sheet (Figure 5). Capacitive sensors maintain the shape of the face sheet with respect to a light weighted Zerodur reference body with ~10 nm precision, at up to a 2 kHz update rate. This internal closed-loop control of the actuators operates at a rate of 90 kHz, and includes dynamic feed-forward control¹⁷. The reference body and actuators are both supported by an aluminum cooling plate, which also provides an interface to the positioner actuators. Six positioner actuators arranged in a modified hexapod connect each segment to the rigid top end structure.

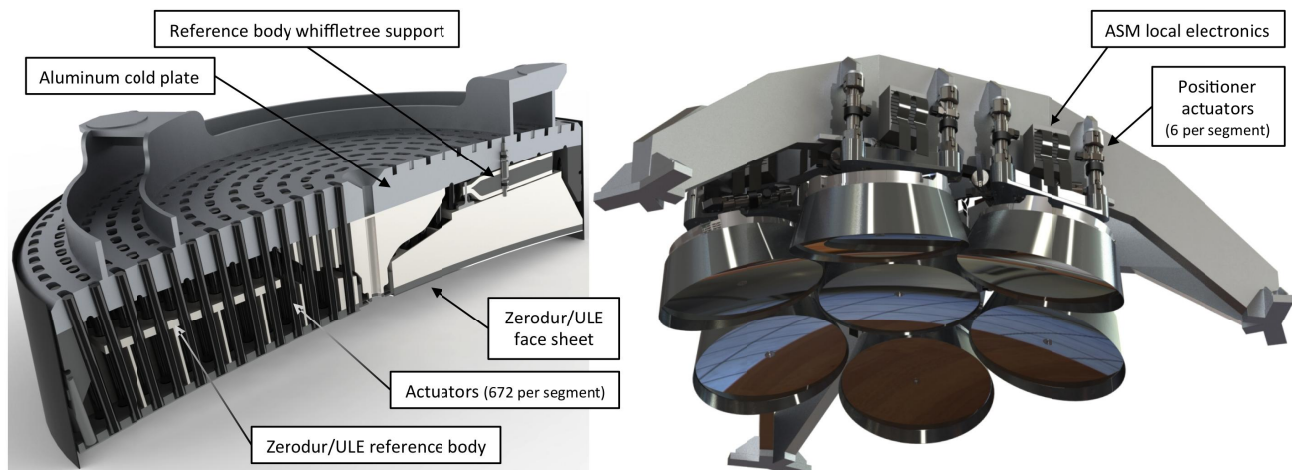


Figure 5. The GMT adaptive secondary mirror, and a cross-section of one off-axis segment.

The 4704 voice coil actuators act on permanent magnets bonded to the rear of the Zerodur face sheets, leading to the desirable property that failed actuators exert no force and can be removed from the control with little reduction in performance. Local control electronics for each segment are housed in cooled crates, which are attached to the top end structure. All global control tasks are performed by the electronics located remotely in the electronics room, which provide the control and data interfaces to the telescope control system.

Once commissioned, the ASM will remain installed for long periods, operate in all operational weather conditions, and support every observing mode. Yearly maintenance campaigns are likely, during which time the FSM would be installed for several weeks, precluding use of the AO observing modes.

3.2 NGAO Mode Wavefront Sensing

The NGAO observing mode will use the light from a single natural guide star, located within 90" of the science target, for wavefront sensing¹⁸. The Natural Guide Star Wavefront Sensor (NGWS) must therefore sense all wavefront aberrations due to the atmosphere and telescope, including tip-tilt, segment piston, and high-order modes. The need to sense segment piston led to the selection of a pyramid wavefront sensor^{19,20}, which also provides high sensitivity and low aliasing properties.

The NGWS components are mounted on a vertically oriented board that patrols the 180" diameter focal plane on two linear stages (Figure 6). Two wavelength channels allow segment piston errors to be measured unambiguously (one 600-850 nm, and the other 850-950 nm). Both cameras sample the GMT pupil with 92×92 subapertures, providing wavefront measurement on approximately the same spatial scales as the ASM actuator spacing. A modal control scheme using Karhunen-Loève modes based the covariance of turbulence in the ASM actuator's command space is used to provide optimal control when using faint guidestars.

A fixed LGS dichroic and a field corrector lens are located just ahead of the NGWS (see Figure 3). The LGS dichroic uses a novel two-element wedged plate design to compensate transmitted aberrations²¹.

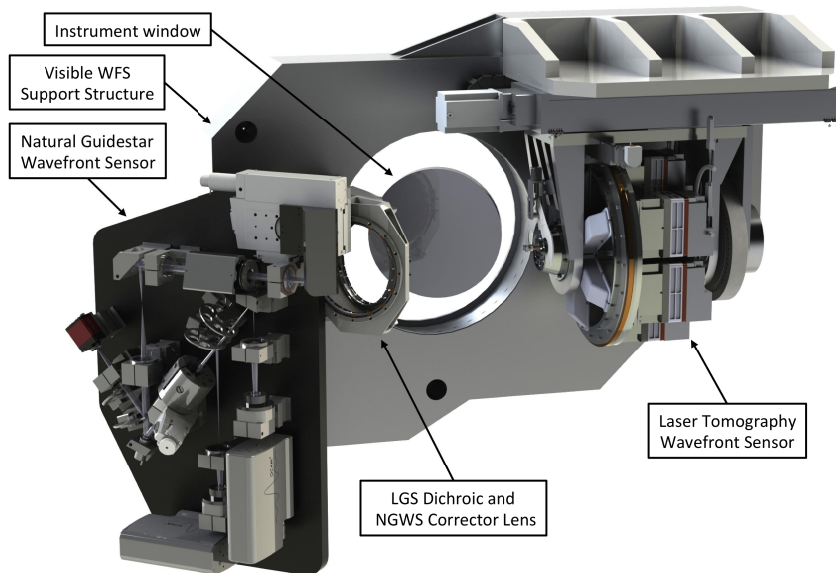


Figure 6. The visible wavefront sensor system, which mounts to the front of diffraction-limited AO instruments.

3.3 LTAO Mode Wavefront Sensing

The Laser Tomography Wavefront Sensor (LTWS) measures the wavefront of the six laser guide stars, allowing the telescope control system in the LTAO observing mode to tomographically reconstruct the high-order components of the atmospheric wavefront aberrations in the direction of a central science target²². The LTWS consists of six Shack-Hartmann wavefront sensors that each divide the GMT pupil into 60×60 subapertures (Figure 6). The spot patterns are recorded by cameras using the E2V NGSD detector, which will operate at up to 800 Hz frame rate. The sensors must translate axially to track the changing range to the atmospheric sodium layer, and rotate around the optical axis to track the laser guide star asterism, which is fixed with respect to the telescope pupil.

Each Shack-Hartmann spot is recorded by 13×13 pixels, critically sampled along the narrow axis of the elongated LGS image ($0.71''/\text{pixel}$). The fine pixel sampling and diversity in the orientation of the LGS elongation result in low LGS aberrations²³. The resulting massive flow of pixels is reduced to a vector of wavefront slopes by a slope processor using 6 commodity multi-CPU servers, which then send the slope vector to the telescope control system via the low-latency data network. Wavefront errors in the direction of the science target and OIWFS natural guide star are estimated using the covariance tomography algorithm²⁴.

Each instrument using the NGAO or LTAO observing modes must provide an OIWFS that observes a single on- or off-axis star, performing different functions depending on the observing mode. In the NGAO mode it compensates flexure, and must therefore measure tip-tilt, focus, and pupil position at slow rates (0.1 Hz). In the LTAO mode, the OIWFS senses all atmospheric and telescope aberrations that cannot be measured with the lasers. These are:

- Tip-tilt of the natural guide star at rates up to 1 kHz in order to compensate for the image motion introduced by the atmosphere, and the wind induced vibration of the telescope
- Focus at rates of approximately 10 Hz, to compensate for sodium layer altitude variations
- Telescope segment piston at 0.1 Hz, to correct slow drifts in the M1 edge sensors
- Low-order aberrations (~ 200 modes) at 0.1 Hz, to detect tomographic reconstruction errors and changing non-common path aberrations

The design of the OIWFS for GMTIFS is illustrated in Figure 7. It has four separate wavefront sensors fed by dichroics, mounted on an optical bench that is in turn mounted to the GMTIFS main optical bench. Tip-tilt sensing is performed using an imaging quad cell in the K-band ($2.03\text{-}2.37 \mu\text{m}$). The H-band is split between a 5×5 Shack-Hartmann focus sensor ($1.65\text{-}1.80 \mu\text{m}$) and an integrated optics phasing sensor²⁵ ($1.50\text{-}1.65 \mu\text{m}$). These three sensors are fed by a small deformable mirror with 32×32 actuators, which corrects the anisoplanatism of the off-axis natural guide star using a separate tomographic solution. A 16×16 subaperture Shack-Hartmann “Truth” wavefront sensor using the J-band ($1.17\text{-}1.33 \mu\text{m}$) is located ahead of the DM²⁶.

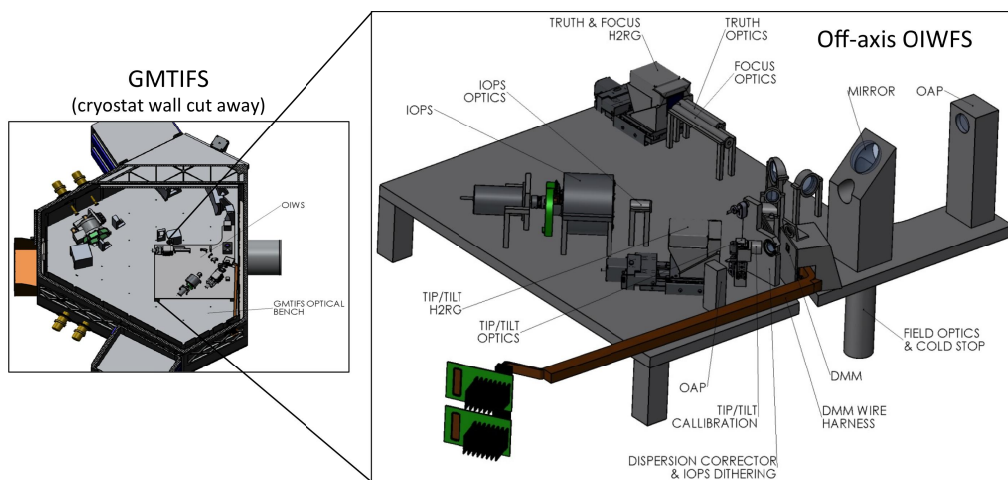


Figure 7. The on-instrument wavefront sensor for GMTIFS.

3.4 GLAO Mode Wavefront Sensing

The Acquisition, Guiding, and Wavefront sensing System (AGWS) fulfills the wavefront sensing function for the GLAO observing mode, in addition to providing telescope guiding, alignment, and M1 segment figure control in the other observing modes²⁷. Four probes patrol the periphery of the direct Gregorian focal plane, each able to access $\pm 90^\circ$ azimuth and from $6'$ to $10'$ radius from 4 cardinal directions (Figure 8). Each probe can be configured in one of three optical configurations: Guider, segment guider (7 subaperture Shack-Hartmann sensor), or wavefront sensor (24×24 subaperture Shack-Hartmann sensor).

In the Natural Seeing (NS) observing mode, one probe will measure segment tilt at up to 200 Hz to correct guiding errors and wind-induced vibration, while three are configured as slow wavefront sensors to maintain M1-M2 alignment

and correct M1 segment figure errors. In the GLAO mode all probes will be configured as wavefront sensors and run at 100-200 Hz, allowing the low-altitude turbulence to be reconstructed and corrected with the ASM. Using a minimum-variance reconstructor that takes into account the position of the guidestars, their magnitude and the size of the science field, image quality can be significantly improved at all wavelengths over fields of view of at least 10' diameter¹², with no throughput reduction or significant additional operational overheads.

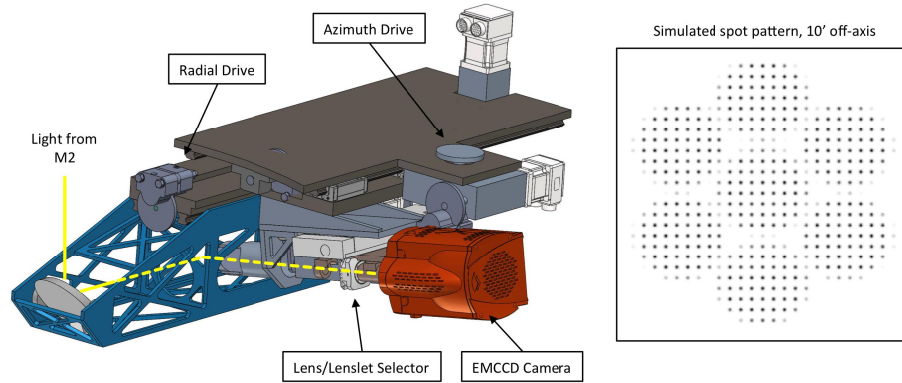


Figure 8. (Left) A single AGWS unit. (Right) AGWS wavefront sensor simulated spot pattern 10' off-axis.

3.5 Laser Guidestar Facility

The laser guide star facility (LGSF) generates the LTAO asterism, which consists of six guide stars equally spaced on a 60 arcsec diameter circle²⁸. Approximately 20 W of optical power per laser is required to generate a return flux $\geq 407 \text{ ph cm}^{-2} \text{ s}^{-1}$ at 15° zenith angle in seasonal minimum sodium conditions ($2.1 \times 10^9 \text{ Na atoms cm}^{-2}$), meeting the LTAO error budget allocation for WFS measurement and bandwidth error.

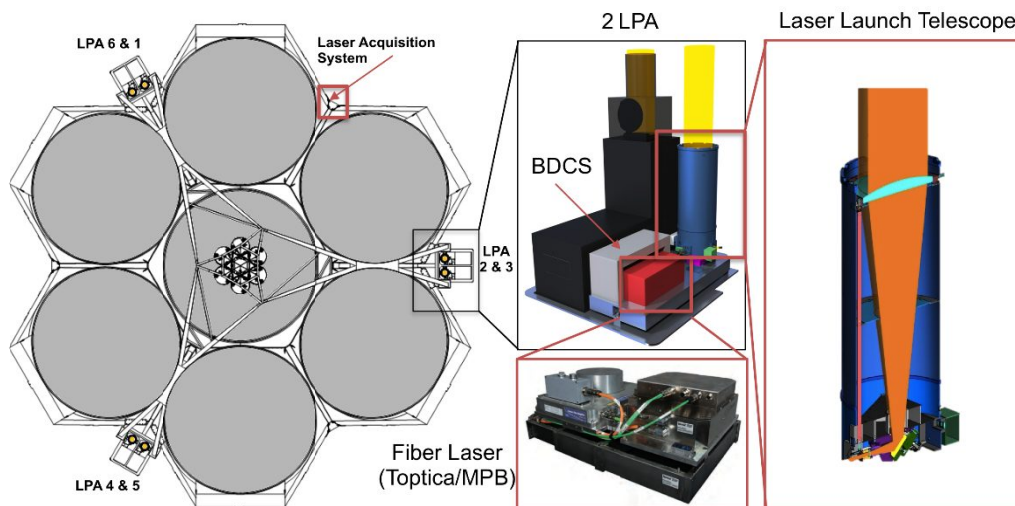


Figure 9. Laser guide star facility components and layout, including the Laser Projection Assembly (LPA), the beam diagnostic and conditioning system (BCDS), fiber laser, and laser launch telescope.

The LGSF uses six self-contained laser guide star units, each of which includes a laser system, a Beam Conditioning and Diagnostic System (BCDS), and a Laser Launch Telescope (LLT) (Figure 9). The baseline laser system is the Toptica/MPB SodiumStar Raman fiber laser, which generates a laser beam with the required power, spectro-temporal, and spatial characteristics in a robust and compact package. This beam is formatted by the BCDS prior to projection on the sky by the LLT. The LLT is a 20× Galilean beam expander designed by TNO for the ESO Very Large Telescope 4LGS Facility, the specifications of which are well matched to those of the GMT. Together, the BCDS and LLT ensure

proper pointing and focusing of the laser beam on the sky. The laser guide star units are located at the periphery of the M1 mirror assembly, mounted in pairs. The location at the end of the M1 cell connector frame provides a very stiff mount and ease of access for maintenance.

An independent laser guidestar acquisition system will be mounted below the M1 cells, on the telescope structure. It will use a commodity 350 mm diameter telescope and CCD camera to image both natural guidestars and the LGS, and open-source starfield recognition software to determine the coordinates of each LGS with respect to the GMT optical axis.

3.6 Segment Phasing

To deliver diffraction-limited images in the NGAO and LTAO observing modes, the GMT must be phased to a small fraction of the observing wavelength. Since both M1 and M2 are segmented, the average optical path of each M1-M2 segment pair must be equalized. The availability of natural guide stars requires a different phasing strategy for the NGAO and LTAO observing modes²⁹.

In the NGAO observing mode, the bright on-axis guide star provides sufficient flux to measure both atmospheric and telescope segment piston at high bandwidth. A pyramid wavefront sensor is capable of measuring phase offsets across segment gaps^{19,20}, but initial simulations and laboratory experiments with a single wavelength sensor exhibited occasional “ejections” of segments to integer multiples of the mean wavelength λ , caused by residual atmospheric turbulence across a segment gap exceeding $\lambda/2$. This effect is common to any sensor using interference effects, even with broadband light. A second channel at a different wavelength was therefore added to the NGWS to detect and correct these jumps. End-to-end simulations of the two-channel NGWS and ASM correction demonstrate the system can meet the 45 nm RMS wavefront error allocated to segment piston in the NGAO observing mode, with no additional sensors.

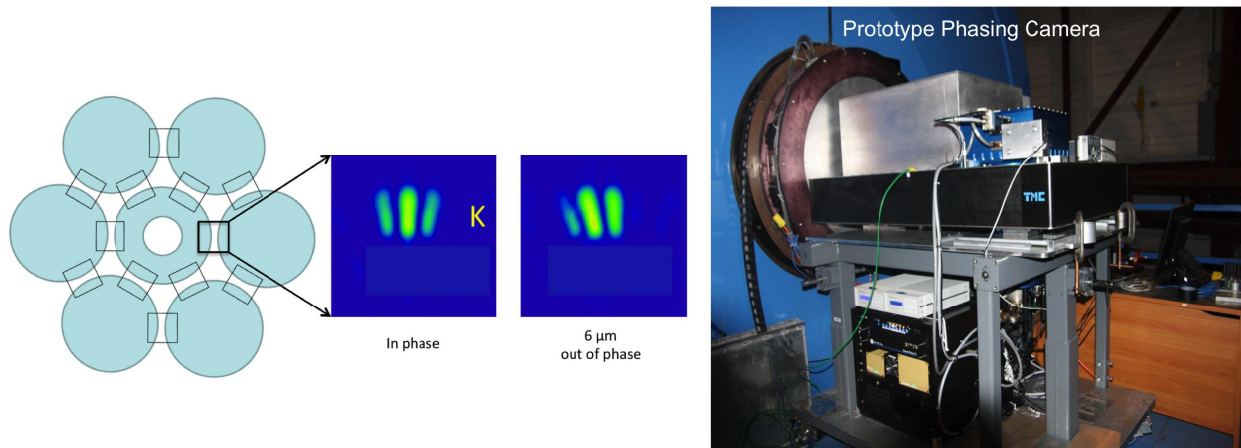


Figure 10. (Left) Phasing camera concept. (Right) Prototype phasing camera on the Magellan Clay telescope in July 2012.

However, there remains an initial capture problem as the NGWS has a capture range of only $\pm 3 \mu\text{m}$, limited by the wavelength separation of its two channels. A separate phasing camera is included in the AGWS for this reason (see Figure 4). The phasing camera uses a dispersed Hartman sensor in the K band to unambiguously determine the segment piston error between adjacent sensors, using NGS located $6'$ to $10'$ off-axis (Figure 10). A prototype was developed and tested on the Magellan Clay telescope in July 2012, demonstrating a piston measurement precision between segment pairs of 75 nm RMS in 30 s using $K=12$ stars, and a capture range of $\pm 60 \mu\text{m}$ ³⁰.

Phasing in the LTAO observing mode is significantly more challenging because the LTWS, being a Shack-Hartmann wavefront sensor, is blind to segment piston errors. Segment piston must therefore be sensed independently of the high-order atmospheric wavefront error, using edge sensors (Figure 11) and faint off-axis NGS. The edge sensors provide high-frequency feedback (≥ 250 Hz) with potential long-term drift due to gravity and thermal effects, while the phasing camera and OIWFS provide continuous low-frequency calibration (typically 30 s integration time).

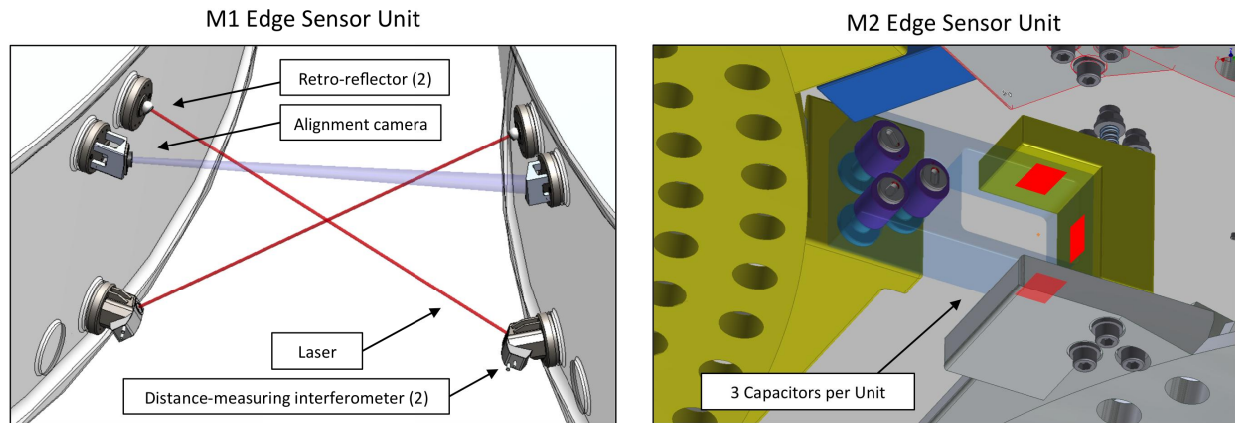


Figure 11. (Left) Each M1 edge sensor unit uses 2 distance-measuring interferometers to measure displacement in 2 directions at each of 24 locations between M1 segments. (Right) Each M2 edge sensor unit uses 3 capacitive sensors across an 0.75 mm gap to measure displacement in 2 directions, at each of 24 locations between the ASM reference bodies.

The phasing camera, while accurately measuring the segment piston at its off-axis position, is subject to field-dependent segment piston errors caused by tilt of an M2 segment compensated by the opposite tilt of the matching M1 segment. This condition results in zero tilt in the focal plane, but a field-dependent segment piston error. Thus the accuracy of the phasing camera measurement is a function of the accuracy to which the M2 edge sensors can maintain relative tilt between the ASM reference bodies. We have therefore also included in the design a sensitive segment piston sensor in the OIWFS²⁵. The Integrated Optics Piston Sensor is located nearer to the optical axis (<90"), and thus subject to an order of magnitude lower field-dependent segment piston error. It also has the advantage of measuring the true average segment piston error, rather than the phase difference over a limited region near the segment edges. Simulations of the LTAO segment piston control loops demonstrate that these sensors used together can maintain telescope segment piston error to 50 nm RMS using IOPS guidestars as faint as H=17, representative of the 20% sky coverage case.

The LTAO phasing strategy can be summarized as:

- Initially phase M2 using the multi-wavelength interferometer reflected by a retro-reflector at the prime focus. Maintain the ASM reference bodies in these relative positions using the M2 edge sensors feeding back to the M2 positioner at ~0.1 Hz.
- Phase M1 using the phasing camera with a bright star in evening twilight. Maintain the M1 segments in these relative positions using the M1 edge sensors feeding back to the M1 segment positioners at ~0.1 Hz.
- Correct the high-frequency component of telescope segment piston by feeding forward the M1 and M2 edge sensor measurements to the ASM segment face sheets at >250 Hz.
- Update the M1 edge sensor setpoints based on continuous IOPS measurements at ~0.1 Hz.

3.7 Wavefront Control System

The Wavefront Control System (WFCS) is the set of TCS software components that implements all active and adaptive optics control for the GMT. It includes all of the software and computing hardware necessary to convert the measurements made by wavefront and edge sensors into corrections applied to the telescope optics. This integrated wavefront control approach is different than that followed by many previous telescope projects in which the AO control system was logically distinct from the telescope control system. The integrated approach, enabled by the concurrent development of telescope and AO systems, avoids the duplication of infrastructure components and facilitates the consistent design of different GMT observing modes.

Each observing mode has a distinct wavefront controller, but all modes share some common software components. Each wavefront controller is instantiated at runtime; the connections between software components are established by a wavefront control supervisor component specific to each observing mode. A top-level wavefront control supervisor implements changes between observing modes.

A single hardware platform will support all first-generation AO wavefront controllers. The LTAO mode places the most demanding requirements on this system, with a throughput requirement of 140 GMACS with $\leq 200 \mu\text{s}$ latency. The baseline design uses 9 commodity servers (Figure 12). Wavefront reconstruction is performed by direct matrix multiplication on 6 of these nodes, each processing the slope vector of one LTWS camera with 3 GPUs (2 for the ASM reconstruction and 1 for the OIWFS DM reconstruction). A master node sums the resultant vectors, and two nodes are dedicated to DM communication. All nodes and the wavefront sensor slope computers communicate via an Infiniband low latency network. A single-node feasibility demonstrator housing 2 GPUs has been developed which demonstrated the required throughput with $225 \mu\text{s}$ latency, slightly out of specification. Anticipated advances in GPUs will likely allow the design to be simplified and performance significantly improved prior to deployment.

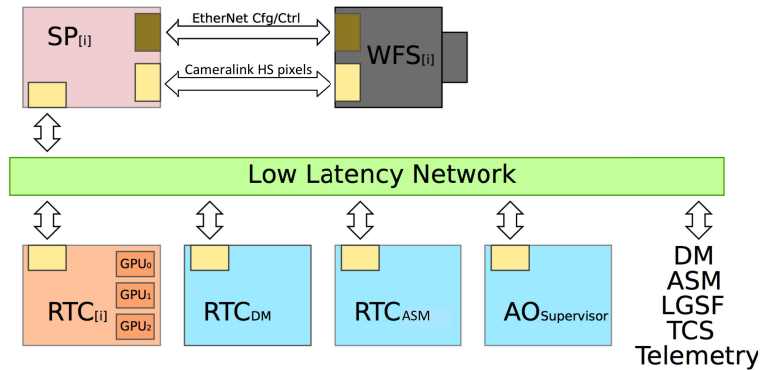


Figure 12. Schematic of the AO wavefront controller hardware architecture. Slope processors (SP) and real-time computer (RTC) nodes are connected via the observatory low latency network to the controlled devices and telemetry system.

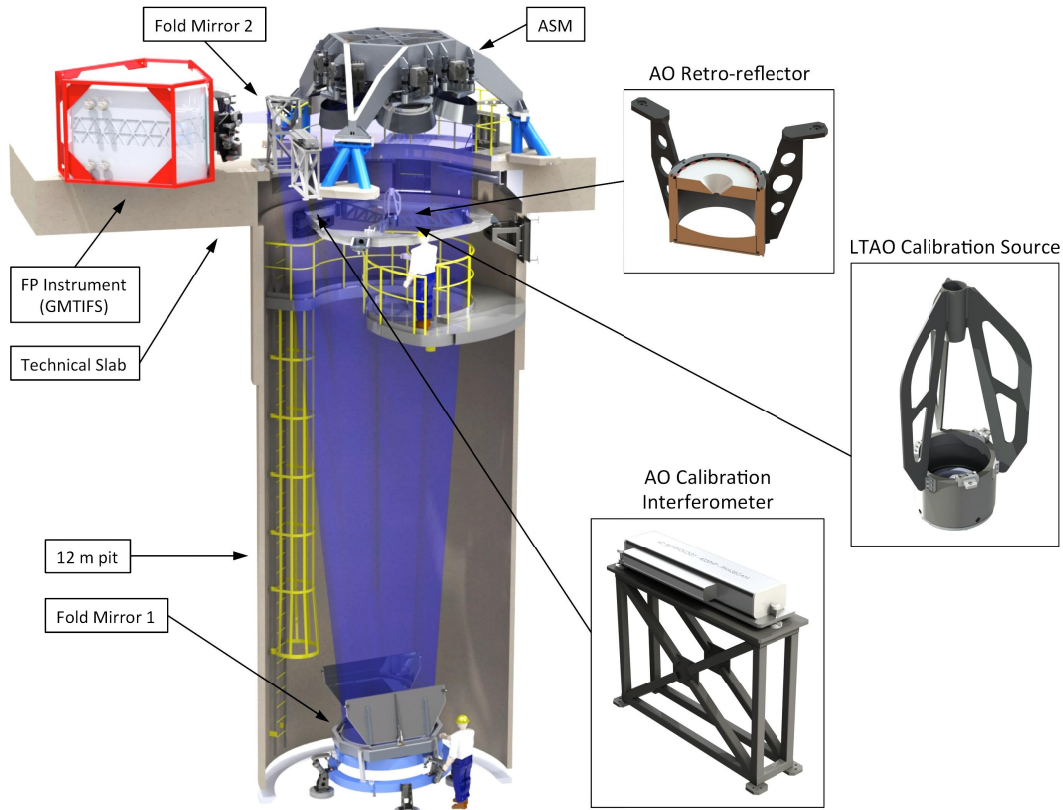


Figure 13. Overview of the M2 Calibration Facility in the Summit Support Building.

3.8 Calibration Systems

Hardware and software systems have been designed to facilitate end-to-end testing of the AO system both on and off the telescope. The M2 Calibration Facility will allow optical testing of the ASM or FSM, integration and system-level testing of the AO system, and integration of the AO system with a folded Gregorian instrument at the observatory (Figure 13). It will be located in the Summit Support Building, 100 m from the telescope enclosure. Two flat fold mirrors, 1.8 m and 0.5 m diameter, fold the optical path from the ASM to an instrument located a grade level in an ISO 8 cleanroom. A 12 m deep pit excavated from bedrock provides both mechanical and temperature stability.

Various sources can be installed at the prime focus. The AO Retro-reflector uses an ellipsoidal and a flat mirror to retro-reflect a source projected from the Gregorian focus while preserving the pupil location. The LTAO Calibration Source uses a computer-generated hologram and a single aspheric optic to simultaneously project NGS and LGS sources to the wavefront sensors and instrument³¹. The second fold mirror can be reoriented to feed a multi-wavelength Twyman-Green interferometer, allowing the ASM optical figure to be measured and the segments phased independent of wavefront or edge sensors.

All of these calibration functions will be available on the telescope as well as in the lab. The prime focus calibration sources will be mounted on a deployment arm, visible in Figure 1 just below the ASM. The calibration interferometer will be mounted in a folded Gregorian instrument location that can be addressed by M3.

4. PREDICTED PERFORMANCE

4.1 Natural Guidestar AO

Simulations of the NGAO observing modes were performed using the software tool PASSATA (PyrAmid Simulator Software for Adaptive OpTics Arcetri) developed at Arcetri Observatory to study pyramid-based AO systems¹⁸. PASSATA is based on a full Fourier optics code including tilt modulation. The ASM correction takes into account the influence functions derived from finite-element analysis of the mirror.

Figure 14 illustrates the rapid convergence of the NGAO control loops for a bright guide star in median turbulence conditions. This simulation used a simple integrator controller and includes no telescope vibrations or calibration errors, and thus represents an upper limit to the system performance. The mean segment piston error over 10 turbulence realizations is 15.3 nm RMS after convergence of the second-wavelength control loop, and the mean K Strehl is 95.6 %.

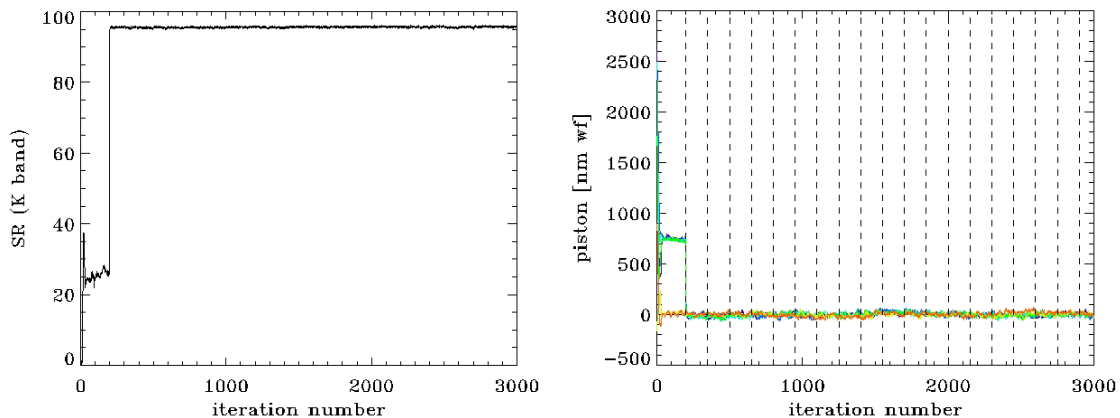


Figure 14. Example of the convergence of the NGAO control loops with a seeing of 0.63" and $V=8$ guidestar. Each iteration represents 1 ms. (Left) K Strehl. (Right) Segment piston error. Vertical dashed lines spaced every 150 ms indicate where second-wavelength channel phasing corrections are applied.

The expected performance of the NGAO mode for various guidestar magnitudes, seeing, and wind conditions is summarized in Table 3. Case D0 represents the requirement (telescope 30° from zenith, pointed into 10 m/s wind, minimum enclosure aperture, 7 mas RMS tip-tilt disturbance), while Case C0 is a worst-case scenario (telescope 30°

from zenith, pointed into 10 m/s wind, wind vents 50% open, 69 mas RMS tip-tilt disturbance). A simple integrator is unable to control tip-tilt and focus in Case C0, and a robust Infinite Impulse Response filter of order (4,4) was therefore used for both wind cases³². An additional 95 nm RMS of wavefront error has been added in quadrature to the simulation results to account for effects not included (eg. calibration errors, uncorrectable telescope and instrument aberrations, residual mechanical vibrations, and flexure).

The expected total wavefront error in the conditions specified in requirement SCI-1883 is 116.1 nm RMS, and the predicted K Strehl is 89.3%. All cases but the most extreme (wind case C0 and an $M_V=12$ guide star) meet the $S_K > 75\%$ criterion.

M_V	Seeing [arcsec]	Wind case	Controller	Wavefront Error [nm RMS]	S_K [%]
8	0.63	none	Integrator	120.9	88.5
		D0	IIR	116.1	89.3
		C0	IIR	122.8	88.1
8	1.0	none	Integrator	154.2	82.0
		D0	IIR	140.9	84.7
		C0	IIR	156.2	81.6
12	0.63	none	Integrator	156.4	81.5
		D0	IIR	133.4	86.2
		C0	IIR	189.9	74.1

Table 3: NGAO mode performance summary.

4.2 Laser Tomography AO

Several AO simulation packages were used to refine the LTAO system design during the preliminary design phase, including the Object Oriented Matlab Adaptive Optics (OOMAO) modeling library³³, the Yorick Adaptive Optics (YAO) simulation tool³⁴, and the Fortran 95 Simulation Library (SL95)²³. The simulation results presented here were computed with SL95 and capture the following key features of the LTAO system:

- 6 LGS in an $r=30''$ hexagonal asterism, plus one off-axis NGS at variable field angle
- LGS point sources convolved by a Gaussian blur kernel, with vertical structure based on UBC lidar sodium density profiles³⁵
- Wavefront reconstruction using a minimum variance tomographic reconstructor, both on-axis (to control the ASM) and off-axis (to control the OIWFS DM)
- Pseudo open-loop control of the ASM and OIWFS DM
- An additional 112 nm RMS of wavefront error to account for error terms not simulated

The image quality metrics of H band Strehl and K band 50×50 mas ensquared energy are displayed in Figure 15 as a function of NGS off-axis distance and magnitude. It is clear from these simulation results that to achieve H Strehl > 0.30 on the science target, a star less than $\sim 60''$ off-axis and with magnitude $H < 16$ must be available for the OIWFS. As expected, the K band 50×50 mas ensquared energy is far less affected by both measurement error and tip-tilt anisoplanatism.

Sky coverage can be estimated by the fraction of 100 random star fields created with the Besançon galaxy model³⁶ with at least one star that delivers a specified image quality. The sky coverage fractions for H Strehl > 0.30 (requirement SCI-1884) and K band 50×50 mas ensquared energy > 0.40 (requirement SCI-1885) are illustrated in Table 4 and Table 5, both with and without an OIWFS DM to correct anisoplanatism of the NGS. The sky coverage without an OIWFS DM formally meets the requirements, but with little margin. That with the OIWFS DM meets both the requirements and the goals, achieving H Strehl > 0.30 over 79% of the sky at the galactic pole, and K band 50×50 mas ensquared energy > 0.40 with complete sky coverage.

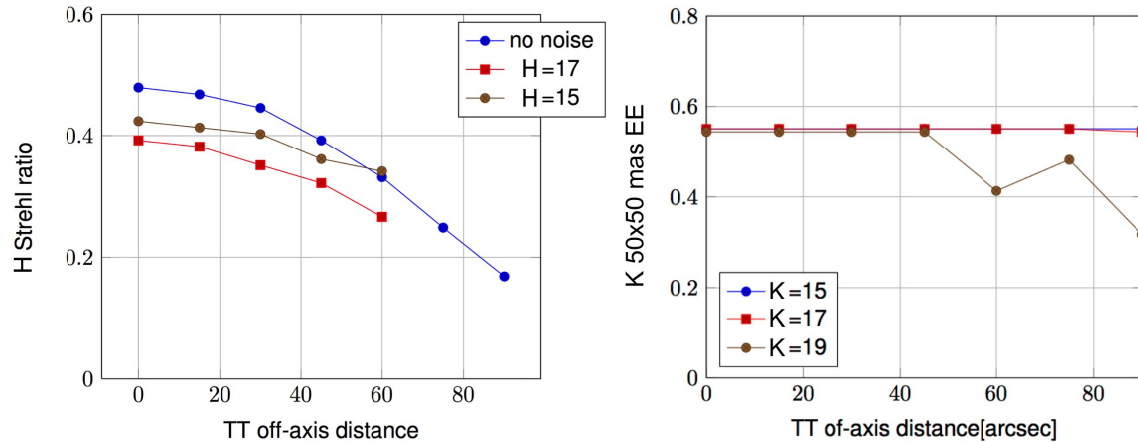


Figure 15. (Left) H Strehl ratio and (Right) K 50×50 mas ensquared as a function of the NGS off-axis distance and magnitude in median seeing. An OIWFS DM correcting anisoplanatism of the NGS is included.

Galactic Latitude	0°	-30°	-60°	-90°
With OIWFS DM	100	100	78	79
Without OIWFS DM	91	51	31	23

Table 4: LTAO sky coverage percentage for H Strehl >0.30 (requirement SCI-1884).

Galactic Latitude	0°	-30°	-60°	-90°
With OIWFS DM	100	100	100	100
Without OIWFS DM	100	95	67	63

Table 5: LTAO Sky Coverage percentage for K 50×50 mas ensquared energy >0.40 (requirement SCI-1885).

The LTAO performance simulations presented above did not include the impact of wind-induced vibrations. These were explored in separate simulations using the same wind cases D0 and C0 described in Section 4.1. Using a simple integrator tip-tilt controller, case D0 resulted in 0.9 mas RMS residual tip-tilt at 20% sky coverage and 1.35 mas RMS at 50% sky coverage at the galactic pole, consistent with the requirements. However, case C0 exceeds the dynamic range of the OIWFS quad-cell detector resulting in tip-tilt residual >6 mas RMS. Future work will explore increasing the dynamic range of the OIWFS tip-tilt sensor, and using more sophisticated control laws to improve performance in these difficult conditions.

4.3 Ground Layer AO

Simulations of the GLAO mode were performed using the Yorick Adaptive Optics (YAO) simulation tool^{13,34}. The simulations include the following features of the GLAO system:

- The current opto-mechanical design of the AGWS, including probe patrol range constraints in field angle (6' to 10') and azimuth ($\pm 90^\circ$).
- Wavefront reconstruction using a minimum variance tomographic reconstructor, optimized for either a single field point, a 5' diameter field, or a 10' diameter field
- Pseudo open-loop control of the ASM

The turbulence profile used is very pessimistic in terms of the fraction of turbulence in the ground layer, with only 28% of the turbulence strength below 1 km altitude. The simulations again used random asterisms generated using the Besançon galaxy model³⁶ to evaluate the performance versus sky coverage. An analytic estimate of the on-axis wavefront error based on the sum of the tomographic error and measurement noise was used to select the optimal asterism in each case.

Tomographic GLAO allows the ASM correction to be optimized for different field sizes or discrete science target locations by changing only the reconstructor. The residual wavefront error for 0', 5', and 10' diameter corrected fields is illustrated in Figure 16 for the median asterism at the galactic pole (that which results in the median on-axis residual wavefront error). For this median case, GLAO correction reduces the atmospheric wavefront error from 2.4 μm RMS uncorrected to 1.0-1.4 μm RMS depending on the corrected field size.

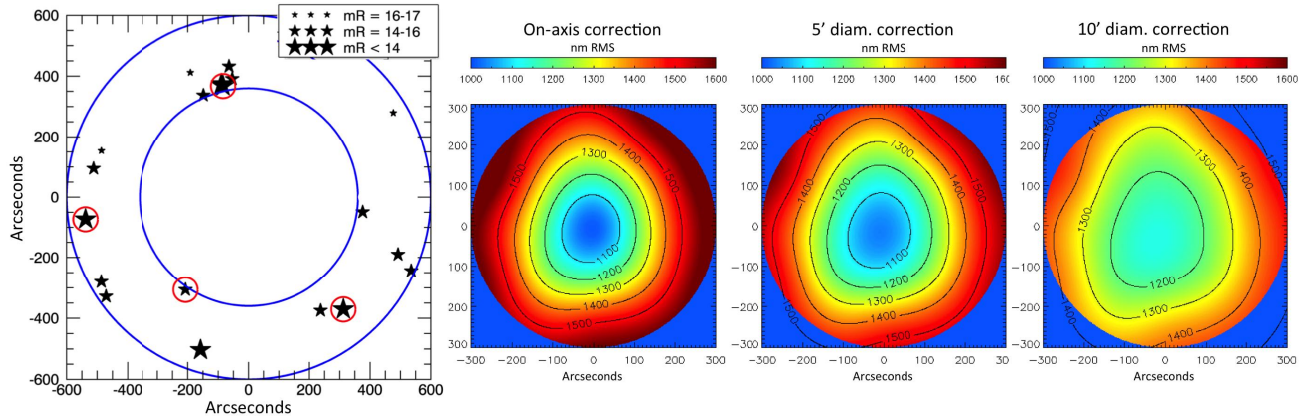


Figure 16. (Left) Median GLAO asterism at the galactic pole. (Right) Residual wavefront error across the central 10' as a function of corrected field size, using the same asterism.

The predicted GLAO image size as a function of wavelength at the galactic pole is illustrated in Figure 17, and tabulated in Table 6. The typical variation in image size between guide star fields is only 1% at visible wavelengths and 3% in the K band, due to the large number of available guide stars, even near the galactic pole. Thus the sky coverage is very nearly 100% at the indicated performance levels. The image size predicted in the natural seeing case is already better than that measured with smaller telescopes in the same atmospheric conditions (0.56 arcsec versus 0.67 arcsec at 550 nm) due to the finite turbulence outer scale. The image quality improvement provided by NGLAO correction is significant at all wavelength bands, increasing with wavelength and smaller corrected fields.

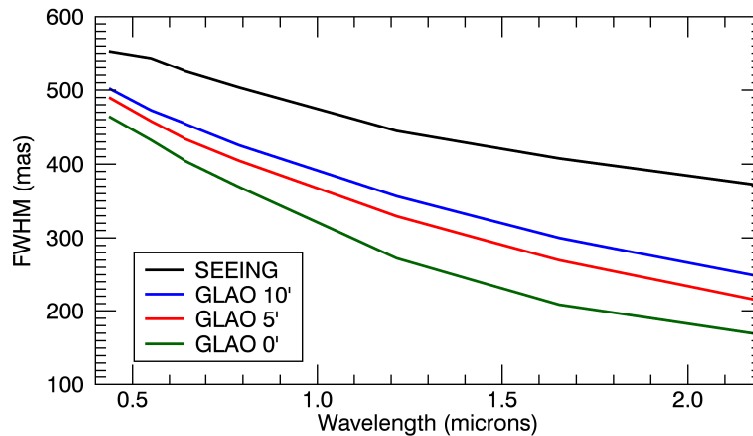


Figure 17. FWHM as a function of wavelength for the on-axis, 5' diameter and 10' diameter corrected fields, for a typical star field near the galactic pole.

Wavelength (μm)	0.44	0.55	0.64	0.79	1.22	1.65	2.18
Natural Seeing (mas)	553	543	526	504	445	408	372
On-axis NGLAO (mas)	463	433	405	369	272	209	169
5' diameter NGLAO (mas)	489	458	435	404	329	270	216
RMS across field (mas)	6.9	7.1	8.4	10.5	10.4	14.6	14.9
10' diameter NGLAO (mas)	501	473	455	425	356	300	249
RMS across field (mas)	7.3	10.4	8.6	10.3	12.6	14.6	18.2

Table 6: GLAO corrected FWHM and FWHM uniformity.

While the improvements in image quality provided by the GLAO mode may appear small, particularly in the visible, they should really be evaluated on the basis of the improvement which they provide in terms of signal-to-noise ratio (SNR) over a given integration time, or reduction in integration time to achieve a given SNR. For background-limited observations of unresolved sources, the SNR will be proportional to $1/\text{FWHM}$. Thus the predicted 17% reduction in R band FWHM over a 5' field provides a 21% increase in SNR, or a 32% reduction in integration time to achieve the same SNR. In this regime, the GLAO mode will provide a great benefit, equivalent to increasing the available observing time on the GMT by nearly 50%. The sensitivity gains in the infrared are even greater.

5. CONCLUSIONS

The GMT AO system passed its preliminary design review in July 2013. The design, presented here, meets all of the top-level performance requirements, and indeed exceeds them in several cases. The NGAO mode in particular is expected to deliver extremely high performance when using bright guidestars (116 nm RMS wavefront error in typical observing conditions, including 10 m/s wind). The LTAO mode sky coverage is effectively 100% for low surface-brightness spectroscopic observations, and greater than 50% for diffraction-limited imaging in the near-infrared. The GLAO mode will provide a significant improvement in observing efficiency, increasing the signal-to-noise ratio of point sources by 30% in the visible and >100% in the near-infrared over wide fields of view.

The construction phase of the GMT is expected to start in late 2014, kicking off detailed design studies and large-scale AO prototyping activities. Fabrication of major AO components will begin in 2016, with integration of the AO subsystems in Chile expected to begin in 2020 and commissioning in 2022. In parallel with these activities, we also plan to begin developing concepts for second generation GMT AO capabilities, coordinated with the second generation of GMT instrument solicitation.

ACKNOWLEDGEMENTS

This work has been supported by the GMTO Corporation, a non-profit organization operated on behalf of an international consortium of universities and institutions: Astronomy Australia Ltd, the Australian National University, the Carnegie Institution for Science, Harvard University, the Korea Astronomy and Space Science Institute, the Smithsonian Institution, The University of Texas at Austin, Texas A&M University, University of Arizona and University of Chicago. This work has also been supported in part by the National Science Foundation under Scientific Program No. 10 as issued for support of the Giant Segmented Mirror Telescope for the United States Astronomical Community, in accordance with Proposal No. AST-0443999 submitted by AURA.

REFERENCES

- [1] Bernstein, R., McCarthy, P., Raybould, K., Bigelow, B., Bouchez, A., Filgueira, J., Gunnels, S., Jacoby, G., Johns, M., Sawyer, D., and Sheehan, M., "Overview and Status of the Giant Magellan Telescope Project", Proc. SPIE 9145-47 (2014).
- [2] Johns, M., Hull, C., Muller, G., Irarrazaval, B., Bouchez, A., Chylek, T., Smith, C., Wadhavkar, A., Bigelow, B., Gunnels, S., McLeod, B., Buleri, C., "Design of the Giant Magellan Telescope," Proc. SPIE 9145-50 (2014).
- [3] Jacoby, G., Bouchez, A., Colless, M., DePoy, D., Jaffe, D., McGregor, P., Sheckman, S., and Szentgyorgyi, A., "The status of the instrument development program for the Giant Magellan telescope," Proc. SPIE 9147-70 (2014).
- [4] McGregor, P. J., Bloxham, G. J., Boz, R., Davies, J., Doolan, M. C., Ellis, M., Hart, J., Nielsen, J. J., Parcell, S., Sharp, R. G. and Stevanovic, D., "The GMT integral-field spectrograph (GMTIFS) conceptual design," Proc. SPIE 8446 (2012).
- [5] Jaffe, D. T., Barnes, S. I., Brooks, C. B., Gully-Santiago, M., Pak, S., Park, C., Yuk, I-S. "GMTNIRS (Giant Magellan telescope near-infrared spectrograph): optimizing the design for maximum science productivity and minimum risk", Proc. SPIE, 9147-74, (2014).
- [6] DePoy, D. L., Allen, R., Li, T., Marshall, J. L., Papovich, C., Prochaska, T., and Schectman, S., "An Update on the Wide Field, Multi-Object, Moderate-Resolution, Spectrograph for the Giant Magellan Telescope", Proc. SPIE 9147-72, (2014).

- [7] Szentgyorgyi, A. et al., “A Preliminary Design for the GMT-Consortium Large Earth Finder (G-CLEF)”, Proc. SPIE 9147-78, (2014).
- [8] Teran, J., et al, “GMT site: facilities and enclosure design overview”, Proc. SPIE 9145-91 (2014).
- [9] Goodwin, M. S., “Turbulence profiling at Siding Springs and Las Campanas Observatories”, Ph.D. Thesis, Australian National University (2009).
- [10] Thomas-Osip, J., Bustos, E., Goodwin, M., Jenkins, C., Lambert, A., Prieto, G., and Tokovinin, A., “Two campaigns to compare three turbulence profiling techniques at Las Campanas Observatory”, Proc. SPIE 7014, 70145I (2008).
- [11] Irarrazaval, B., Buleri, C., and Johns, M., “Wind response of the Giant Magellan Telescope”, Proc. SPIE 9150-77 (2014).
- [12] Hinz, P. M., Brusa, G., Vaitheeswaran, V., McMahon, T., Connors, T., Knox, R., Bouchez, A., and Montoya, M., “Design and predicted performance of the GMT ground-layer adaptive optics mode”, Proc. SPIE 8447, 74473R (2012).
- [13] van Dam, M. A., Bouchez, A. H., and McLeod, B. A., “Wide field adaptive optics correction for the GMT using natural guide stars”, Proc. SPIE 9148-38 (2014).
- [14] Riccardi, A., et al., “Adaptive secondary mirrors for the Large Binocular Telescope”, Proc. SPIE 7736, 77362C (2010).
- [15] Close, L., et al., “High Resolution H α Images Of The Binary Low-Mass Proplyd Lv 1 with the Magellan AO System”, Ap. J. 774, 45 (2013).
- [16] Biasi, R., et al., “VLT deformable secondary mirror: Integration and electromechanical tests results”, Proc. SPIE 8447, 84472G (2012).
- [17] Manetti, M., Morandini, M., and Mantegazza, P., “Servo-fluid-elastic Modeling of Contactless Levitated Adaptive Secondary Mirrors”, Computational Mechanics 50, 85–98 (2012).
- [18] Esposito, S., Pinna, E., Quiros-Pacheco, F., Puglisi, A. T., Carbonaro, L., Bonaglia, M., Biliotti, V., Antichi, J., Briguglio, R., Agapito, G., Arcidiacono, C., Riccardi, A., and Fini, L., “Design, prototyping and numerical simulations of the GMT natural guide star WFS”, Proc. SPIE 9148-91 (2014).
- [19] Ragazzoni, R., “Pupil plane wavefront sensing with an oscillating prism”, J. Modern Optics 43, 289-293 (1996).
- [20] Esposito, S., et al., “Pyramid sensor for segmented mirror alignment”, Optics Letters 30, 2572-2574 (2005).
- [21] Antichi, J., Pinna, E., Esposito, S., Bonaglia, M., Busoni, L., Santoro, F. G., Bouchez, A. H., “Meaningful options for a dichroic unit within the natural & laser guide star AO systems at the Giant Magellan telescope”, Proc. SPIE 9148-189 (2014).
- [22] Conan, R., Bennet, F., Bouchez, A. H., van Dam, M. A., Espeland, B., Gardhouse, W., d'Orgeville, C., Parcell, S., Piatrou, P., Price, I., Rigaut, F., Trancho, G., and Uhlendorf, K., “The Giant Magellan Telescope laser tomography adaptive optics system”, Proc. SPIE 8447, 84473P (2012).
- [23] Piatrou, P. K. and Conan, R., “Integrated modeling of the GMT laser tomography adaptive optics system”, Proc. SPIE 9148-247 (2014).
- [24] Conan, R., “Fast iterative optimal estimation of turbulence wavefronts with recursive block Toeplitz covariance matrix”, Proc. SPIE 9148-26 (2014).
- [25] Bennet, F., Uhlendorf, K., Gardhouse, R., Conan, R., Espeland, B., and Bouchez, A., “Integrated optic segment piston sensor for the GMT”, Proceedings of the Third AO4ELT Conference (2013).
- [26] van Dam, M. A., Conan, R., Bouchez, A. H., and Espeland, B., “Design of a truth sensor for the GMT laser tomography adaptive optics system”, Proc SPIE 8447, 844717 (2012).
- [27] McLeod, B., Bouchez, A. H., Espeland, B., Figueira, J., Johns, M., Norton, T. J., Ordway, M., Podgorski, W. A., Roll, J., and Smith, C., “The Giant Magellan Telescope active optics system”, Proc. SPIE 9145-64 (2014).
- [28] d'Orgeville, C., Bouchez, A., Conan, R., Espeland, B., Gardhouse, R., Hart, J., Price, I., Trancho, G., and Uhlendorf, K., “GMT Laser Guide Star Facility”, Proceedings of the Third AO4ELT Conference (2013).
- [29] Bouchez, A. H., McLeod, B., and Acton, D. S., “The Giant Magellan Telescope phasing system”, Proc. SPIE 8447, 84473S (2012).
- [30] Kanneganti, S., McLeod, B. A., Ordway, M. P., Roll, J. B., Shtetman, S. A., Bouchez, A. H., Codona, J., Eng, R., Gauron, T. M., Handte, F., Norton, T. J., Streechon, P., and Weaver, D., “A prototype phasing camera for the Giant Magellan Telescope”, Proc. SPIE 8447, 844752 (2012).
- [31] Zhou, P., Burge, J. J., Zhao, C., Benjamin, S. D., Cuerden, B., Bouchez, A. H., “Design of adaptive optics calibration source for the Giant Magellan telescope”, Proc. SPIE 9148-192 (2014).

- [32] Agapito, G., Arcidiacono, C., Quiros-Pacheco, F., Puglisi, A., and Esposito, S., “Infinite Impulse Response Modal Filtering in Visible Adaptive Optics”, Proc. SPIE 8447, 844731 (2012).
- [33] Conan, R., and Correia, C. M., “Object-oriented Matlab adaptive optics”, Proc. SPIE 9148-248 (2014).
- [34] Rigaut, F., “YAO::home”, <<http://frigaut.github.io/yao/>> (2014).
- [35] Pfrommer, T. and Hickson, P., “High resolution mesospheric sodium properties for astronomical applications”, Astronomy & Astrophysics 565, A102 (2014).
- [36] Robin, A. C., Reylé, C., Derrière, S., and Picaud, S., “Synthetic View on Structure and Evolution of the Milky Way”, Astron. & Astrophys. 416(1), 157 (2004).